Stress-dependent design and optimization methodology of gradient porous implant and application in femoral stem

Changning Sun[a,b], Jianfeng Kang[c], Ling Wang[a,b], Zhongmin Jin[a,d], Chaozong Liu[e] and Dichen Li[a,b]

[a]State Key Laboratory for Manufacturing System Engineering, School of Mechanical Engineering, Xi'an Jiaotong University, Xi'an, ShaanXi, China; [b]National Medical Products Administration (NMPA) Key Laboratory for Research and Evaluation of Additive Manufacturing Medical Devices, Xi'an, ShaanXi, China; [c]Jihua Laboratory, Foshan, Guangdong Province, China; [d]School of Mechanical Engineering, University of Leeds, Leeds, UK; [e]Division of Surgery & Interventional Science, University College London, Royal National Orthopaedic Hospital, London, UK

ABSTRACT

Gradient porous structure made by additive manufacturing (AM) technology is potential to improve the long-term stability of orthopaedic implants through bone ingrowth while maintaining mechanical safety. In this study, a parametrical optimization methodology for the customized gradient porous implants was developed based on a stress-dependent design algorithm. Clinical requirements and manufacturing capabilities of AM were considered in the design procedure. A femoral stem with a minimum bone loss proportion of 2.4% by optimizing the control parameters. This study provided a feasible and flexible design approach for the customized implant with gradient porous structure or material components.

KEYWORDS

Gradient porous implant; elastic modulus; finite element analysis; customized implant; additive manufacturing

1. Introduction

Prosthesis with gradient porous structure could offer combined mechanical and biological properties, therefore, it was widely used in orthopaedic fields (Han et al. 2019; Zadpoor 2019; Murr 2020). Additive Manufacturing (AM) allows the production of controllable porous structures with features that are conducive to bone ingrowth and has become the most applicable manufacturing method for gradient porous implants. The design of the porous structure determines the success of the prosthesis and has become one of the most popular topics in the applications of gradient porous prosthesis. In the design, gradient porous prosthesis is regarded as functional gradient material (FGM) whose composition and/or microstructure vary smoothly in space (Sola et al. 2016). The basic idea of FGM parts is to optimize the material properties instead of the design of material components or microstructure based on understanding the relationship between the microstructure/material components and the macroscopic mechanical properties.

In the optimization of mechanical properties of FGM implants, reduction of stress shielding, reduction of shear stress on the bone-implant interface, prevention of bone absorption and wear resistance of articular surface were selectively used as the optimization objectives. The works from the literature on the design of FGM implants in recent years are summarized in Table 1. The application of functional gradient design in orthopaedic implants was first proposed by Huiskes et al. (Kuiper and Huiskes 1997), by whom the stress conduction of implant was increased by distributing different materials in different locations. In the early stage, the two-dimensional conceptual finite element (FE) model was commonly used due to the limitation of computing power. As such, Hedia et al. (Hedia et al. 2014, 2019) carried out lots of research on designing artificial hip joints to reduce the shear stress on the bone-prosthesis interface and stress shielding. Three-dimensional (3 D) FE models had to be used in the design of prostheses with complex geometries. For example, the elastic modulus of the femoral condyle in the artificial knee joint was optimized by 3 D finite element analysis (FEA) to improve the wear resistance of the articular surface and lower the stress shielding effects according to Bahraminasab et al. (2014). However, the geometry-dependent distribution pattern of elastic modulus or relative density in FGM design was an essential limitation of these studies. For example, the elastic modulus of the

Table 1. Recent literature on the design of FGM prosthesis.

Application	Reference	Benefits from FGM	Distribution Pattern of Elastic Modulus
Cementless Femoral Stem	Wang et al. (2018); Arabnejad et al. (2017)	a) Minimizing bone resorption b) Mechanical Safety c) Interface failure	Implant was discretized with 75 sampling points on the medical-lateral plane of the femoral stem.
Cement Femoral Stem	Moussa et al. (2017)	a) Minimizing bone resorption b) Cement damage	Implant was partitioned along proximal-distal and medial-lateral axes.
Cervical fusion cage	Moussa et al. (2018)	a) Minimizing subsidence	Global stiffness matrix.
Cementless Femoral Stem	Wang et al. (2020)	a) Minimizing bone resorption b) Micro-motion on the interface	Implant was partitioned along the proximal-distal axis and radially.
Intervertebral Disc Prosthesis	Jiang et al. (2019)	a) Motion range of Intervertebral disc b) Stress of implant	Disc prosthesis was modeled as a graded shell structure divided into 50 layers radially.
Cementless Femoral Stem	Alkhatib et al. (2019)	a) Minimizing bone resorption b) Micro-motion on the interface	Implant was partitioned along the proximal-distal axis.

femoral stem was optimized along the stem axis, the relative density of the acetabulum cup was defined as a function of its radius. The predefined distribution pattern was proved to be effective in designing implants with simple geometry but might be limited in the implants with complex geometry such as pelvic reconstruction prosthesis and mandibular implant. Therefore, novel optimization methods to get rid of the geometry-dependent distribution pattern of material properties were studied. Pasini et al. (Arabnejad et al. 2017; Wang et al. 2018) developed a gradient-free algorithm that considered bone resorption, fatigue safety and interface failure to optimize the relative density distribution of a femur stem. (Ait Moussa and Yadav 2017; Arabnejad et al. 2017; Moussa et al. 2018; Alkhatib et al. 2019; Jiang et al. 2019; Wang et al. 2020).

The following criteria should be considered in the design of gradient porous implants, including the strength safety, suitable porosity and pore size for the bone ingrowth, avoiding stress shielding, manufacturing constraints and time spent on the designing. However, different criteria were embodied as contradictory requirements in the design of the porous implant, typically the implant with suitable porosity and pore size was lack of strength(Liu et al. 2021), and the fine microstructure also challenged the capabilities of AM technology. In order to resolve the contradictory requirements, design algorithms that can comprehensively concern clinical requirements and manufacturing constraints needed to be developed. In addition, the design algorithm would be expected to be adaptive so that it can be employed in customized prostheses.

Focusing on the design of gradient porous implant, an adaptive design algorithm of gradient elastic modulus was reported by a previous study (Sun et al. 2018) and demonstrated in the design of the femoral stem. Safety and stress shielding were quantified in a FE model and set as design criteria in the optimization algorithm. In the optimization, a stress-depend-ent distribution was first used in the gradient elastic modulus design, breaking through the limitation of the geometry-dependent distribution pattern. However, the shortcoming was that the elastic modulus of the implant was defined as linearly correlated with the stress distribution. Thus, the distribution of elastic modulus of the implant could not be adjusted accurately to obtain quality results. Therefore, the investigation of the modulus-stress relationship in the design algorithm becomes necessary to obtain an implant with a gradient porous structure that is more in line with the biomechanical requirements.

This study aims to investigate the effect of the modulus-stress relationship in the adaptive design algorithm of the gradient elastic modulus on the biomechanical performance of the implant. A parametric control methodology of the modulus-stress relationship was established by taking a femoral stem as a typical example. Control parameters were optimized based on the design criteria of implant safety, early-stage bone-implant healing, and long-term stability of the implant. The study provided an adaptable and flexible design methodology for gradient porous implants.

2. Materials and methods

2.1. Design methodology of elastic modulus distribution

The multi-scale design methodology that led to the development of gradient implant with a controllable porous structure that minimizes stress shielding and guarantees safety was summarized in Figure 1. A patient-specific FE model consisting of a typical

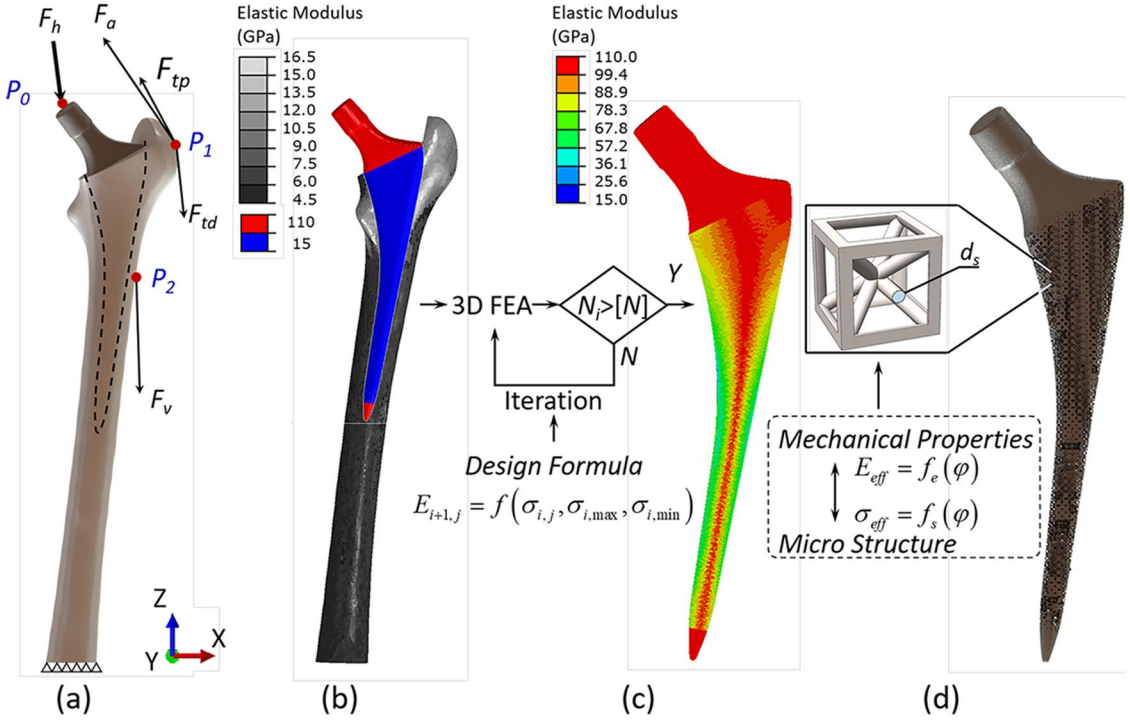

Figure 1. Multi-scale design framework of gradient porous implant. (a) Three-dimensional finite element model. F_h——hip joint force; F_a, F_{tp}, F_{td}, F_v——muscle forces. (b) Initial setting in the design procedure of elastic modulus distribution of implant. (c) Gradient elastic modulus distribution of femoral stem. (d) 3 D model of the gradient porous implant constructed from the gradient elastic modulus distribution*.

Note*: The 3D model of the femoral stem of Figure 1d was an example of porous gradient femoral stem with another RVEs instead of BCC to demonstrate the design framework of the porous implant but not the real photo of the product.

uncemented femoral stem and proximal femur was established, and the details of the modeling are described in the Supplemental File 1. Algorithms were introduced into the model (Figure 1(a)) to adjust the elastic modulus distribution of the femoral stem(Sun et al. 2018). In the beginning, the elastic modulus of the design domain was set as similar as cortical bone (Figure 1(b)). The modulus of elements in the design domain was changed during the iterations to meet the safety requirement. Gradient porous implant with controllable structure was then constructed on the foundation of the relationship(Wang et al. 2017) between mechanical properties (equivalent elastic modulus and yield strength) and microstructure of a type of representative volume elements (RVEs). RVEs with body-centered cubic (BCC) structure were employed as a demonstration, and the mechanical properties and the corresponding geometry parameters of the BCC structure were detailed in Supplemental File 2.

2.2. Univariate analysis

The above-mentioned femoral stem was composed of FGMs with variable mechanical properties based on the stress itself. During the iterations in the design procedures of the mechanical properties of the implant, a stress-based algorithm was developed to assign elastic modulus for the implant according to the following Equation (1):

$$E'_{i+1,j} = \begin{cases} \left(1 - \frac{r'_{i,j} - b}{1-b}\right)^g, & r'_{i,j} > b,\ Element_j \notin Element_{Surf} \\ 1, & r'_{i,j} \le b,\ Element_j \notin Element_{Surf} \\ E_j = E_{Surf}, & Element_j \in Element_{Surf} \end{cases} \quad (1)$$

where i denotes iteration cycle; j denotes element number; $E_{i+1,j}$' denotes the relative elastic modulus of element j in the next iteration; $r_{i,j}$' denotes the relative von Mises stress of element j in the iteration i; g denotes relative modulus-stress gradient exponent; b denotes relative stress threshold of porous element (%); E_j denotes the elastic modulus of element j in every iteration; E_{Surf} denotes the elastic modulus of the elements near the surface, i.e. the element set named $Element_{Surf}$.

The definitions of relative von Mises stress and elastic modulus are as following Equations (2) and (3):

$$r'_{i,j} = \frac{r_{i,j} - r_{i;min}}{r_{i;max} - r_{i;min}} \quad (2)$$

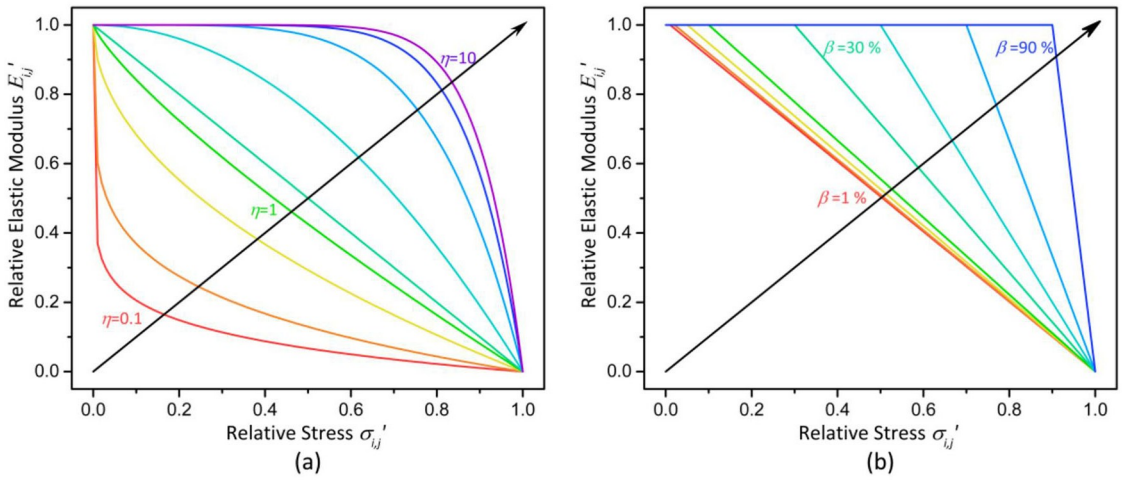

Figure 2. Relationship between Element elastic modulus and stress (a) Different values of g = 0.1, 0.2, 0.5, 0.8, 1, 2, 5, 8 and 10 When b = 0%; (b) Different values of b = 1%, 2%, 5%, 10%, 30%, 50%, 70%, and 90% when g = 1.

$$E'_{i+1,j} = \frac{E_{i+1,j} - E_{min}}{E_{max} - E_{min}} \tag{3}$$

where $r_{i,j}$ denotes the stress of element j from iteration i; $r_{i,max}$ and $r_{i,min}$ denote the maximum and minimum value of the stress at the regions of interest of the prosthesis; $E_{i+1,j}$ denotes the elastic modulus of element j in iteration $i + 1$; E_{max} and E_{min} denote the maximum and minimum limits of usable elastic modulus, for titanium alloy E_{max} = 110 GPa and E_{min} = 15 GPa.

Relative elastic modulus $E_{i+1,j}$' varying with relative stress $r_{i,j}$' are presented in Figure 2 for different g and b. The variation of relative modulus-stress gradient exponents (g) affected the relationship between the relative elastic modulus in the next iteration and the relative stress of each element in current iterations. For example, an element whose relative stress is 0.5, would be given a new relative modulus of 0.07, 0.5 and 0.99 with different g of 0.1, 1 and 10, respectively. b was a threshold that controlled the proportion of solid elements during the iterations. Elements whose relative stress is lower than b % would be assigned a relative modulus of 100% which meat the elastic modulus of solid material. Elements belonging to the set {$Element_{Surf}$} were assigned with a constant elastic modulus of E_{surf} but not influenced by other parameters. As presented in Figure 2, univariate research was carried out without the consideration of surface elements to investigate the effect of g and b on the processes and results in the designing of elastic modulus distribution. E_{Surf} was changed from 1 GPa to 110 GPa when g = 1 and b = 0%, to study the effect of surface modulus on the designing processes and results.

2.3. Multivariate analysis

To search for the optimal parameters of designing the elastic modulus distribution of implant, a multi-objective optimization problem was formulated as:

$$\begin{aligned} &find\ b = \ g,\ b,\ E_{Surf}\ ; \\ &min:\ \ f(b) = x_1 \cdot V_{BL}(b) + x_2 \cdot T(b); \\ &S.\ t.:\ N \geq 10 \end{aligned} \tag{4}$$

where the vector b denotes the design variables which consisted of g, b *and* E_{surf}, each parameter in vector b had seven available values (see Table 2); f (v) is the multi-objective function; $V_{BL}(b)$ denotes the volume fraction of bone with density loss which was assessed by the comparison of strain tensor of host bone before and after implantation on the foundation of Huiskes' bone adaptation law; $T(b)$ denotes the total iteration times which reflects the design efficiency; x_1 and x_2 denote the weight of V_{BL} and T, x_1+x_2 =1; N denotes the global safety of the implant. Refer to the previous study of the authors for the numerical calculation method of N and V_{BL}(Sun et al. 2018).

In this optimization problem, the remodeling of surrounding bone and design efficiency were integrated as one objective function by different weight ratios x_1 and x_2. The global safety factor, calculated by the minimum value of local safety factors of all elements, was set as a constraint to guarantee that any gradient elastic modulus or porous structure obtained by the optimization algorithm meets the safety requirements. Furthermore, the global safety factor was applied as the termination condition to guarantee the safety of the implant.

Table 2. The value of parameters in design variables b=(g, b, E_{surf}).

Relative Modulus-Stress Gradient Exponent (g)	Relative Stress Threshold of Porous Element (b/%)	Elastic Modulus of the Elements Near the Surface (E_{surf}/GPa)
0.1	1	1
0.2	2	2
0.5	5	5
1	10	8
2	30	11
5	50	14
10	90	17

3. Results

3.1. Univariate analysis

The final global safety factors (N), solid volume proportions (P_{Solid}/%), modulus of surface elements in the design domain (E_s/GPa), the volume of bone with density loss (V_{BL}/%) along with the iteration times (T) required to the design procedure of elastic modulus distribution, were all affected by the controlling parameters namely relative modulus-stress gradient exponent (g), relative stress threshold of porous element (b/%) and elastic modulus of surface elements (E_{Surf}) as presented in Figure 3.

The variation of relative modulus-stress gradient exponent (g) had a significant influence on the solid volume proportions and iteration times but did not affect the final global safety factors (Figure 3(a)). The increased g reduced the iteration times when g ≥ 0.8, but only one or two iterations were demanded when g < 0.8. Solid elements were the elements whose elastic modulus was larger than 100 GPa in the design domain. The volume proportion of solid elements (P_{Solid}) increased with g. The modulus of surface elements (E_S) as well as bone loss proportion (V_{BL}) shows a similar tendency (Pearson correlation coefficient R^2=0.9981) with the variation of g as presented in Figure 3(b). The volume of bone with density was 2.8% when g = 0.1 and rose to 13.2% when g = 10, the corresponding modulus of surface elements was 26.3 ± 17.5 GPa and 105.8 ± 4.4 GPa, respectively.

As shown in Figure 3(c), the required iterations times were lower with the larger relative stress threshold of porous element (b), especially when b = 50%, 70% and 90%, the design procedures were terminated at the first iterative calculation. The global safety factors of the designed gradient implant were just above 10 when b ≤ 50%. The terminal condition of the design procedures for the elastic modulus distribution was that the global safety factor of the implant at a certain iteration met the requirement of allowable safety factor [N] = 10. Even so, the global safety of the designed femoral stem was approximately 20 when b = 70% and 90%, in which cases the implant was almost solid. Solid proportion (P_{Solid}) increased after fell firstly along with the raise of b and the minimum value was 25% appeared at b = 5%. Similar trends were found in modulus of surface elements (E_S) and bone loss proportion (V_{BL}) (Figure 3(d)) with solid proportion in the design domain.

An obvious difference in iteration times and solid proportion was obtained by the design with E_{Surf} larger or less than 15 GPa. The solid proportion was 0% and iteration times was 0 when $20 \le E_{Surf} \le 90$ GPa, while P_{Solid} = 26 ~ 34% and T = 8 ~ 10 when $E_{Surf} \le 15$ GPa (Figure 3(e)). The implant model under initial condition met the safety requirement of $N_0 > [N]$, so the iteration times were 0 when $E_{Surf} \ge 20$ GPa. The solid proportion was 32% when E_{Surf} = 110 GPa but all the solid elements were near the surface, and the global safety factor was 24.2. The elastic modulus of the elements below the outer layer surface (E_S) were all set to be 15 GPa when $E_{Surf} >$ 15 GPa before the iteration starts, but the bone loss proportions (V_{BL}) were increased to 6.3% under these conditions. And when $E_{Surf} \le 15$ GPa, the values of E_S and V_{BL} were similar.

The elastic modulus distributions on a sagittal section of femoral stem designed by different g, b and E_{Surf} are presented in Figures 4–6, respectively. The modulus distribution in Figures 4 and 5 shows similar feature that the regions with higher modulus was in funnel-shaped and elastic modulus reduced gradually from the inside out. In Figure 6, elastic modulus distribution in the non-surface region in the design domain is gradient when $E_{Surf} \le 15$ GPa but are homogeneous when $E_{Surf} > 15$ GPa. Conversely, the elastic modulus in the surface region was constant depending on input values.

3.2. Multivariate analysis

The three controlling parameters of elastic modulus distribution were optimized via an orthogonal test in seven levels. Analysis of variance (ANOVA) and F-test were performed under different weight ratios of the objective functions. When x_1=1 and x_2=0, i.e. $f(b)=V_{BL}(b)$, the F-value of g, b and E_{Surf} were F_g= 16.92, F_b= 5.02 and F_E=0.10, respectively. Thus g and b had significant impacts ($F_{0.005}$=3.95) on the volume of bone with density loss of gradient implant. Conversely, when x_1=0 and x_2=1, i.e. $f(b)=T(b)$, F_g= 3.43, F_b= 13.81 and F_E=1.35, which reflected that only b had significant impact on iteration times.

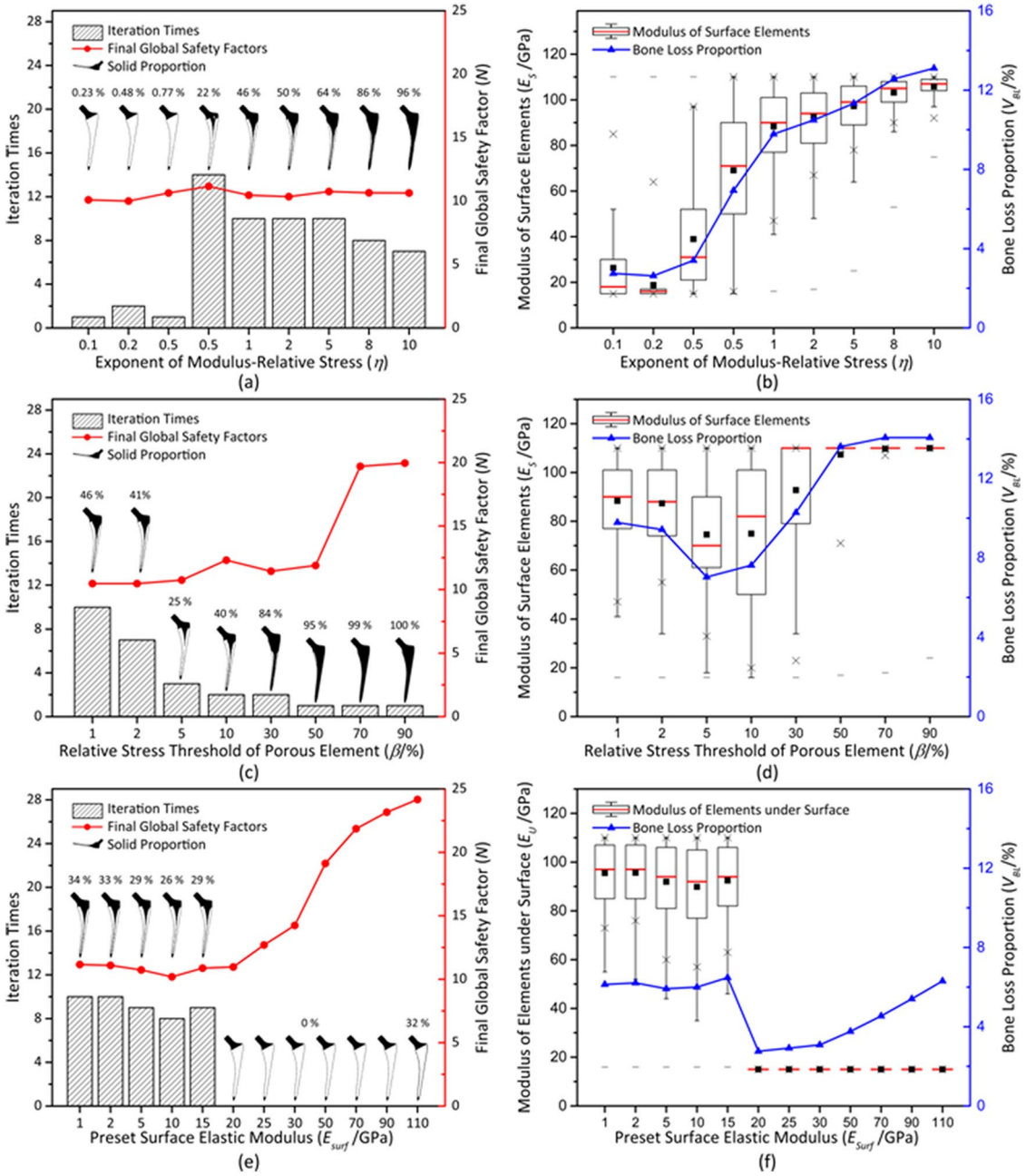

Figure 3. The influence of g, b and E_{surf} on the processes and results in the designing of elastic modulus distribution. The effect of exponent of the relationship between modulus and relative element stress (g) on: (a) iteration times, final global safety factor and solid proportion, (b) surface modulus and bone loss proportion. The effect of relative stress threshold of porous element (b/%) on (c) iteration times, final global safety factor and solid proportion, (d) surface modulus and bone loss proportion. The effect of elastic modulus of surface elements (E_{Surf}) on: (e) iteration times, final global safety factor and solid proportion, (f) surface modulus and bone loss proportion.

The relationships between bone loss proportion (V_{BL}) and iteration times (T) corresponding significant factors were presented in Figure 7. Smaller values of g and b were beneficial to reducing bone loss proportion while a higher value of b could contribute to shorting iteration times required by the design of elastic modulus distribution.

The optimal design variable b= (g, b, E_{Surf}) was set b_V=(0.2, 5%, 5 GPa) and b_T=(0.1, 30%, 8 GPa) for the objective function of $f(b)=V_{BL}(b)$ and $f(b)=T(b)$. Results were obtained by performing the multi-scale design procedure of gradient implant using both parameters. There is a great difference between the calculated elastic modulus of the two gradient femoral

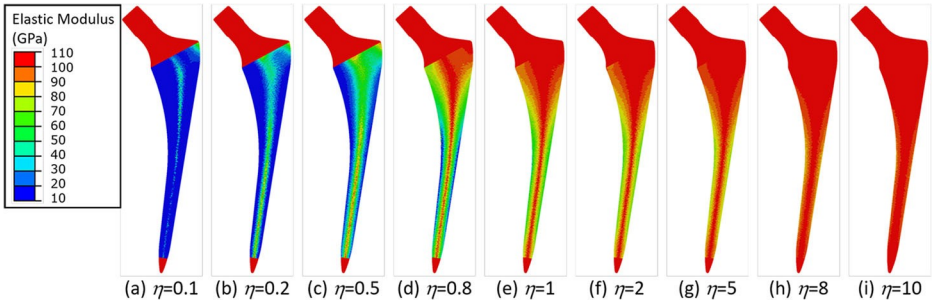

Figure 4. The elastic modulus distributions of femoral stem on different exponent of the relationship between modulus and relative element stress (g).

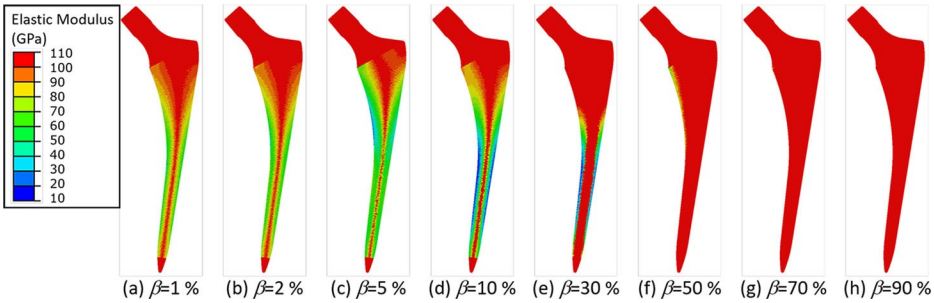

Figure 5. The elastic modulus distributions of femoral stem on different relative stress threshold of porous element (b/%).

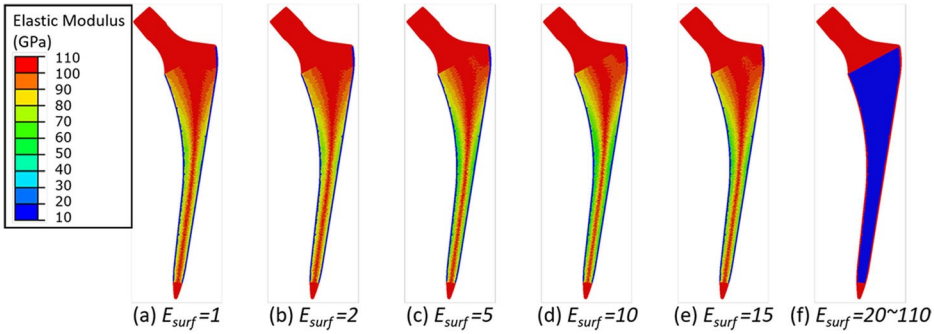

Figure 6. The elastic modulus distributions of femoral stem on different Elastic Modulus of Surface Elements (E_{surf} /GPa).

stems as shown in Figure 8(a) and 8(c). As presented in Figure 8(b) and 8(d), the stress at the implant designed by variable b_V is much less than those designed by b_T.

The von Mises stress at the surrounding femur of the two femoral stems are presented in Figure 9(a). The stress on the internal surface of the medullary cavity were counted and the frequency chart were shown in Figure 9(b), the overall stress of the medullary cavity of stem b_V were larger than those of b_T. The level of the bone loss was assessed by S/S_{ref}, where S was the strain tensor of the element in the femoral model with implant and S_{ref} was the strain tensor of a completely healthy femur. The smaller the S/S_{ref} becomes, the more bone loss was expected at a certain location. The bone loss of the femur with femoral stem b_V was 2.4%, less than half of the femur with stem b_T (Figure 9(c)). The major difference was the bone loss near the proximal femur was relieved by stem b_V comparing to those of stem b_T.

4. Discussion

In the present study, a parametric control method of the modulus-stress relationship was established based on the adaptive design methodology of the elastic modulus of gradient porous implant. The optimal control parameters were obtained by employing the bone loss proportion and iteration times as objective functions in the optimization procedure. Results indicated that the modulus-stress gradient exponent (g)

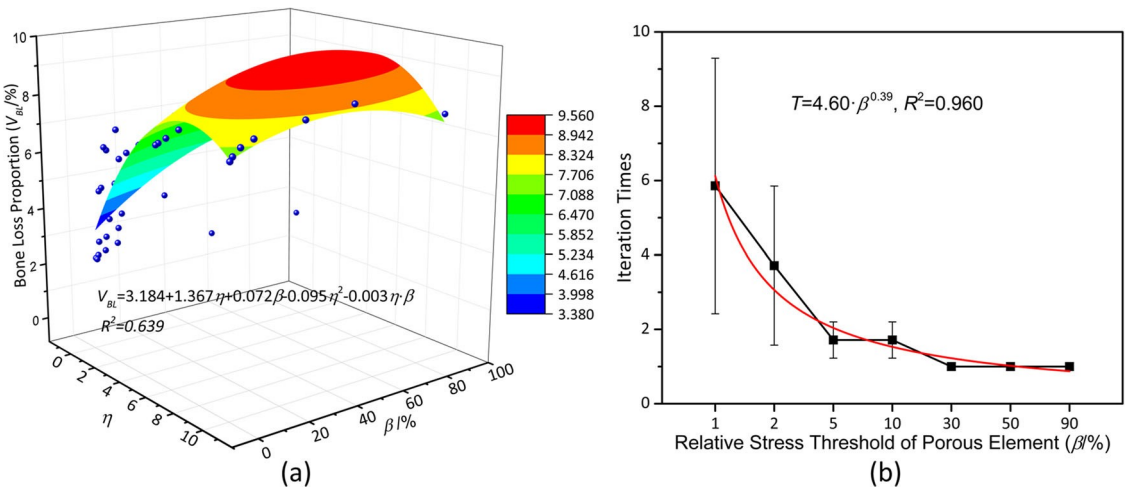

Figure 7. (a) The effect of exponent of the relationship between modulus and relative element stress (g) as well as relative stress threshold of porous element (b) on bone loss proportion (V_{BL}/%). (b) The effect of relative stress threshold of porous element (b) on iteration times.

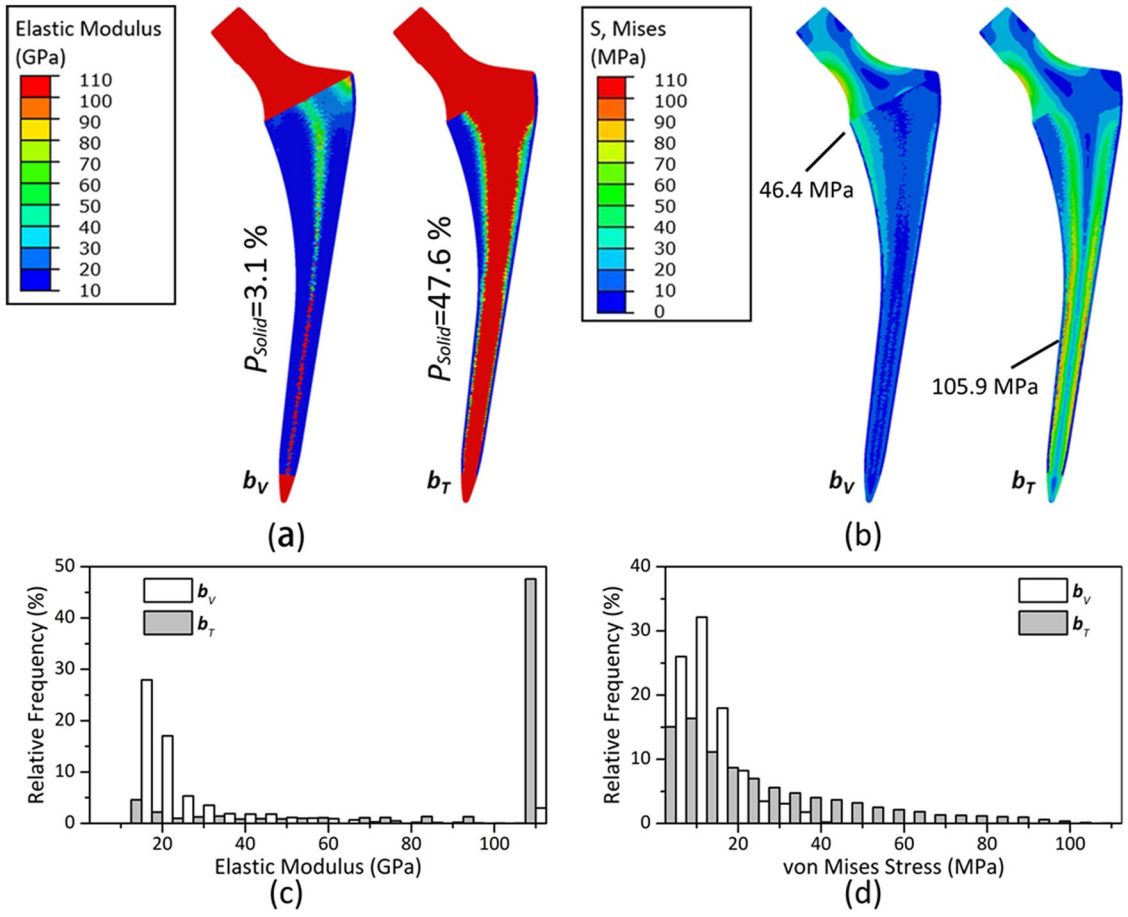

Figure 8. Elastic modulus distribution and stress of the gradient hip stem designed by using b_V=(0.2, 5 %, 5 GPa) and b_T=(0.1, 30 %, 8 GPa). (a) Elastic modulus distribution; (b) Stress pattern; (c) Frequent count of elastic modulus in non-surface region of the design domain; (d) Frequent count of von Mises stress in the design domain.

has the most significant impact on the bone loss proportion while the relative stress threshold of porous element (b) affected the iteration times and subsequently determined the processing time required for the optimizing design. The bone loss proportion of the surrounding bone of the femoral stem was reduced to 2.4% through the parametric optimization developed in the present study.

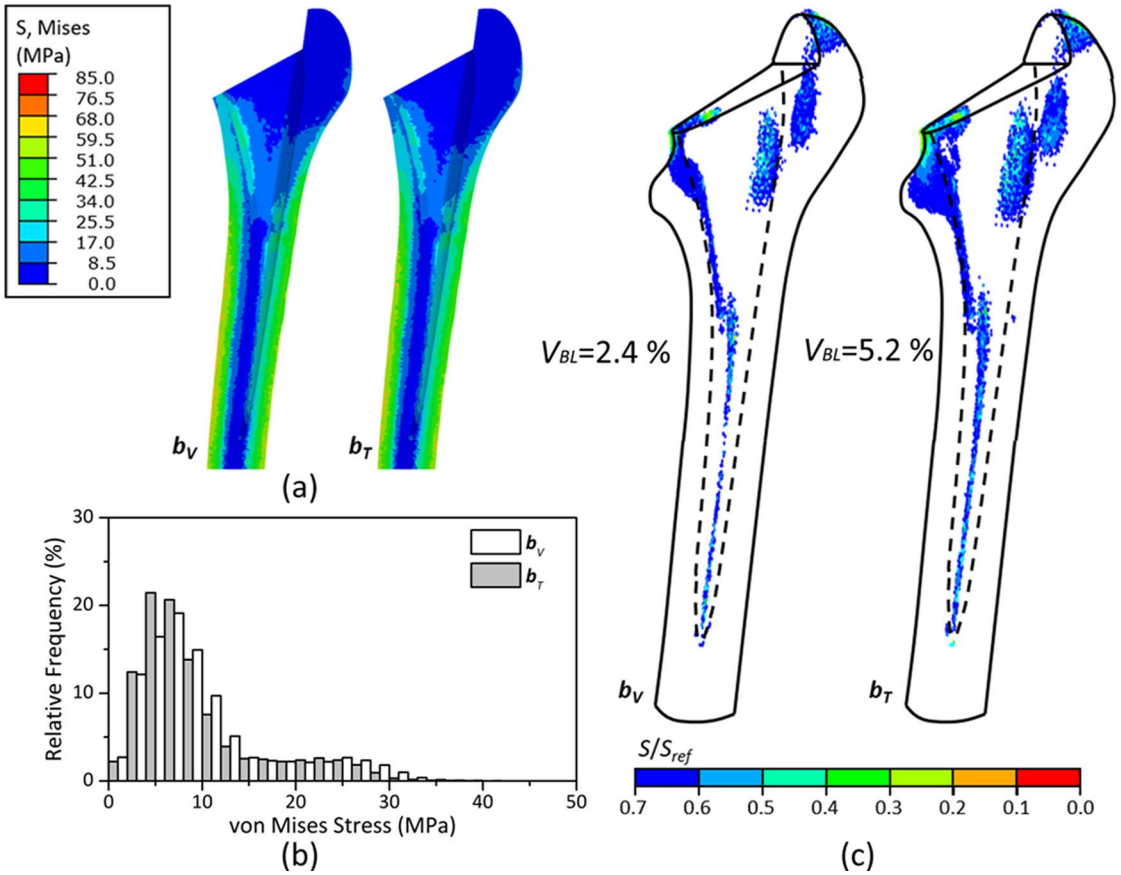

Figure 9. Stress and bone loss of the surrounding bone implanted with the gradient hip stem designed by using b_V=(0.2, 5 %, 5 GPa) and b_T=(0.1, 30 %, 8 GPa). (a) von Mises stress of the bone; (b) Frequent count of von Mises stress of elements on the internal surface of femoral marrow cavity; (c) 3 D diagrams with color dots representing the location with density loss in the femurs for different gradient stem.

Clinical and engineering requirements of porous implants were translated to quantifiable design criteria in the numerical simulation and optimization as follows:

a) Global safety factor (N) was applied to quantified the safety of the implant with gradient porous structure and was set as a boundary condition of the optimization. It depended on the understanding of constitutive equations relating microstructure to macro mechanical properties, including elastic modulus and yield stress or failure stress, as well as an accurate stress distribution of FGM implants. As it was difficult to measure the stress or strain field of an FGM implant, FEA was used to predict the stress distribution of the optimized FGM femoral stem, while the mechanical properties were driven by experimental results from a previous study. This prediction of the safety of the optimized femoral stem may not be entirely accurate, as the stress obtained by FEA was not validated by the experiment. Therefore, a large allowable global safety factor was used to alleviate the uncertainty in the safety of the implant caused by the potential errors in the FEA.

It is hard to quantify the safety of implants due to the lack of constitutive equations in the design of FGM implants from early research. Safety could be quantified based on understanding the constitutive equations of porous structure so that FGM implant could be truly realized.

Bone ingrowth is the key to the osseointegration of the porous implants. Porosity and pore size were believed to play important roles in the bone ingrowth of the metal porous structure. The porosity and pore size near the surface should be in the proper range to achieve the early-stage healing between bone and porous implant by bone ingrowth. The suitable porosity is 50%~80% and the

applicable pore size is in the range of 200 ~ 500 lm (Bose et al. 2013; Taniguchi et al. 2016; Wang et al. 2016; Kapat et al. 2017; Zhu et al. 2020). The elastic modulus close to the interface between implant and bone was limited to 1 ~ 17 GPa, which is similar to that of the bone. The corresponding porosity was about 40–90% if it is made of Ti6Al4V (Yanez et al. 2018; Kang et al. 2020), and is consistent with the demand of bone ingrowth into the porous structure(Sobral et al. 2011; Wang et al. 2018; Li et al. 2020).

Bone loss proportion is one of the objective functions of the optimization procedure in this study. Aseptic loosening induced by bone loss is the primary failure reason of metal orthopaedic implants (Li et al. 2018). The enormous stiffness incompatibility ini-tialed the stress shielding and eventually caused the periprosthetic bone loss. Porous structure was an effective way to decrease the stiffness of metal implants but would cause loss of strength incidentally. The loss of surrounding bone was minimized by optimizing gradient porous structure with the premise of safety as the boundary condition (Wang et al. 2021; Zhang et al. 2021).

Manufacturing feasibility was usually disregarded in many studies of the design of FGM implants. Currently, Powder-Bed Fusion (PBF), also known as Selective Laser Melting or Electronic Beam Melting, was one of the mainstream methods to manufacture metal parts in AM technology. PBF manufactured the parts by selectively melting the metal powder on the powder bed using a laser or electron beam as a heat source. There were two constraints from PBF for the manufacture of porous structures: on the one hand, RVEs with structs dimensions were too small to be accurately formed, which was influenced by different factors represented by the laser spot size (Sing et al. 2018). On the other hand, the pore size must not be too small so that the residual unmelted powder cannot be effectively removed. In order to meet both constraints, the minimum elastic modulus was set to 15 GPa in the optimization algorithm, which allows the corresponding diameter of the struct to be no less than 480 lm, based on the Equation (S2-6). On the other hand, the relative stress threshold of the porous elements (b/%) was set as a control parameter setting the elements whose relative elastic modulus was higher than b as solid to avoid the difficulty of powder removal with minor porosity or high relative elastic modulus.

In the reconstruction surgery of bone defects caused by trauma or tumors, which were the main applications of AM prosthesis, the time spent on the design process should be limited to meet the timeliness of the surgery. Therefore, the iteration times representing the time spent was used as one of the objective functions.

Three control parameters, g, b, and E_{surf}, were used to acquire the optimal elastic modulus distribution of the femoral stem. Among them, g decided the relationship between elastic modulus of each element and its relative stress in the implant, thus showing the most significant effect on the elastic modulus distribution of the target implant and directly affected the biomechanical performance of bone and implant. Optimization with lower g acquired an implant with smoother gradient distribution of elastic modulus, in which maximum stress is lower since the stress concentration caused by the large gradient of elastic modulus was eased. b mainly controlled the volume of the solid elements in the implant during the iterations. These solid elements with high elastic modulus and strength were the key to the bearing capacity of the implant, thus the increase of b resulted in higher global safety factors and a decrease in iteration times. A large value of b should be avoided because of the low porosity, redundant safety factors and high bone loss volume of the designed implant. E_{surf} showed neither effect on the stress of bone and implant, nor contributed to the stress conduction of implant to the bone. Therefore, the determination of the surface elastic modulus and geometric features of the porous structure near the surface should follow the factors required for bone ingrowth such as porosity, pore size and structs size, instead of the influence on the stress distribution of the bone and implant. It is worth noting that the elastic modulus of the elements below the outer layer surface was all optimized to the minimum value of 15 GPa, which produced a hollow hip stem that was comparable in the inhibition of the bone loss to that the gradient porous implant with high internal modulus and low surface modulus. This hollow-like implant was very similar to the topological optimized hollow implant obtained by Tan et al. (Tan and van Arkel 2021), which also found that the hollow femoral stem obtained a weaker stress shielding effect and sufficient strength. A hollow-like femoral stem was obtained by both gradient porous optimization of this paper and topological optimization from Tan et al. (Tan and van Arkel 2021), which may suggest that a hollow femoral stem could be an option in the future.

Optimal parameters of g, b and E_{surf} were selected with different weight ratios of V_{BL} and T by

multivariate analysis. The dilemma from different design criteria was compromised by using an objective function with variable weight ratios. However, it should be noted that these optimal parameters were only applicable to one type of implant, thus for other implants, similar optimization procedures would be required to determine the corresponding optimal parameters.

There remain several limitations in this study. First, instead of carrying out experimental tests on the manufactured gradient porous femoral stem, the stress distribution and the safety of the optimized femoral stem was assessed based on the understanding of the mechanical properties of RVEs obtained from experiments results of published work. Lacking of the direct experimental validation is one of the limitations of this study. Second, the manufacturabil-ity of optimized femoral stem with gradient porous structure need to be confirmed in the future study. Third, only a RVEs of BCC and femoral stem were employed as a demonstration of the optimization method, the potential of the method for other prostheses and RVEs was not demonstrated.

In future perspective, the stress-dependent optimization procedure developed in this study needs to be used in other prostheses and be validated by physical experiments. Another essential prospect is developing the design software or programs based on the optimization methodology in this study to make it more clinic accessible.

5. Conclusion

A design methodology of implants with gradient mechanical property and its parametrical optimization procedure was developed in this study. The conflicting requirements of different design criteria for porous prosthesis were taken into account in the design of implant with gradient mechanical properties through the rational arrangement of control parameters, boundary conditions and objective function. A femoral stem was taken as an example, a minimum bone loss proportion of 2.4% was aimed for by the optimal control parameters. Compared with current research on gradient design of orthopaedic implants, the clinical requirements were considered more comprehensively in the optimization and design algorithm in this study, thus providing a feasible and flexible design approach for the customized implant with gradient porous structure.

Disclosure statement

No potential conflict of interest was reported by the authors.

Funding

The work was supported by the National Key R&D Program of China [2018YFE0207900], Key R&D Program of Guangdong Province [2018B090906001], China Postdoctoral Science Foundation [2020M683458], Key R&D Program of Ningxia Province [2020BCH01001], the Natural Science Basic Research Program of ShaanXi Province [grant number 2022JQ-378], the Program of the National Natural Science Foundation of China [51835010], the Fundamental Research Funds for the Central Universities [XZY012021007] and the Youth Innovation Team of Shaanxi Universities.

References

Ait Moussa A, Yadav R. 2017. Optimization of a functionally graded material stem in the femoral component of a cemented hip arthroplasty: influence of dimensionality of FGM. J Med Eng. 2017:3069351.

Alkhatib SE, Tarlochan F, Mehboob H, Singh R, Kadirgama K, Harun WSB. 2019. Finite element study of functionally graded porous femoral stems incorporating body-centered cubic structure. Artif Organs. 43(7):E152–E164.

Arabnejad S, Johnston B, Tanzer M, Pasini D. 2017. Fully porous 3D printed titanium femoral stem to reduce stress-shielding following total hip arthroplasty. J Orthop Res. 35(8):1774–1783.

Bahraminasab M, Sahari BB, Edwards KL, Farahmand F, Hong TS, Arumugam M, Jahan A. 2014. Multi-objective design optimization of functionally graded material for the femoral component of a total knee replacement. Mater Des. 53:159–173.

Bose S, Vahabzadeh S, Bandyopadhyay A. 2013. Bone tissue engineering using 3D printing. Mater Today. 16(12): 496–504.

Han Q, Wang CY, Chen H, Zhao X, Wang JC. 2019. Porous tantalum and titanium in orthopedics: a review. ACS Biomater Sci Eng. 5(11):5798–5824.

Hedia H, Aldousari S, Abdellatif A, Fouda N. 2014. A new design of cemented stem using functionally graded materials (FGM). Biomed Mater Eng. 24(3):1575–1588.

Hedia HS, Aldousari SM, Timraz HA, Fouda N. 2019. Stress shielding reduction via graded porosity of a femoral stem implant. Mater Test. 61(7):695–704.

Jiang QF, Zairi F, Frederix C, Yan Z, Derrouiche A, Qu ZW, Liu XB, Zairi F. 2019. Biomechanical response of a novel intervertebral disc prosthesis using functionally graded polymers: A finite element study. J Mech Behav Biomed Mater. 94:288–297.

Kang J, Dong E, Li D, Dong S, Zhang C, Wang L. 2020. Anisotropy characteristics of microstructures for bone substitutes and porous implants with application of additive manufacturing in orthopaedic. Mater Des. 191: 108608.

Kapat K, Srivas PK, Rameshbabu AP, Maity PP, Jana S, Dutta J, Majumdar P, Chakrabarti D, Dhara S. 2017. Influence of porosity and pore size distribution in Ti6Al4V foam on physicomechanical properties, osteogenesis and quantitative validation of bone ingrowth by micro-CT. ACS Appl Mater Interfaces. 9(45): 39235–39248.

Kuiper JH, Huiskes R. 1997. Mathematical optimization of elastic properties: application to cementless hip stem design. J Biomech Eng. 119(2):166–174.

Li J, Cui XL, Hooper GJ, Lim KS, Woodfield TBF. 2020. Rational design, bio-functionalization and biological performance of hybrid additive manufactured titanium implants for orthopaedic applications: a review. J Mech Behav Biomed Mater. 105:18.

Li ZH, Muller R, Ruffoni D. 2018. Bone remodeling and mechanobiology around implants: insights from small animal imaging. J Orthop Res. 36(2):584–593.

Liu BW, Xu W, Lu X, Tamaddon M, Chen MY, Dong JQ, Liu YT, Guo LJ, Zhang JZ, Qu XH, et al. 2021. The optimization of ti gradient porous structure involves the finite element simulation analysis. Front Mater. 8:11.

Moussa A, Tanzer M, Pasini D. 2018. Cervical fusion cage computationally optimized with porous architected Titanium for minimized subsidence. J Mech Behav Biomed Mater. 85:134–151.

Murr LE. 2020. Metallurgy principles applied to powder bed fusion 3D printing/additive manufacturing of personalized and optimized metal and alloy biomedical implants: an overview. J Mater Res Technol-JMRT. 9(1): 1087–1103.

Sing SL, Wiria FE, Yeong WY. 2018. Selective laser melting of lattice structures: A statistical approach to manufacturability and mechanical behavior. Rob Comput Integr Manuf. 49:170–180.

Sobral JM, Caridade SG, Sousa RA, Mano JF, Reis RL. 2011. Three-dimensional plotted scaffolds with controlled pore size gradients: effect of scaffold geometry on mechanical performance and cell seeding efficiency. Acta Biomater. 7(3):1009–1018.

Sola A, Bellucci D, Cannillo V. 2016. Functionally graded materials for orthopedic applications - an update on design and manufacturing. Biotechnol Adv. 34(5): 504–531.

Sun CN, Wang L, Kang JF, Li DC, Jin ZM. 2018. Biomechanical optimization of elastic modulus distribution in porous femoral stem for artificial hip joints. J Bionic Eng. 15(4):693–702.

Tan N, van Arkel RJ. 2021. Topology optimisation for compliant hip implant design and reduced strain shielding. Materials. 14(23):7184.

Taniguchi N, Fujibayashi S, Takemoto M, Sasaki K, Otsuki B, Nakamura T, Matsushita T, Kokubo T, Matsuda S. 2016. Effect of pore size on bone ingrowth into porous titanium implants fabricated by additive manufacturing: An in vivo experiment. Mater Sci Eng C Mater Biol Appl. 59:690–701.

Wang L, Kang J, Sun C, Li D, Cao Y, Jin Z. 2017. Mapping porous microstructures to yield desired mechanical properties for application in 3D printed bone scaffolds and orthopaedic implants. Mater Des. 133:62–68.

Wang P, Li XW, Luo SM, Nai MLS, Ding J, Wei J. 2021. Additively manufactured heterogeneously porous metallic bone with biostructural functions and bone-like mechanical properties. J Mater Sci Technol. 62:173–179.

Wang S, Li RY, Li DD, Zhang ZY, Liu GC, Liang HJ, Qin YG, Yu JH, Li YY. 2018. Fabrication of bioactive 3D printed porous titanium implants with Sr ions-incorporated zeolite coatings for bone ingrowth. J Mater Chem B. 6(20):3254–3261.

Wang S, Zhou X, Liu L, Shi Z, Hao Y. 2020. On the design and properties of porous femoral stems with adjustable stiffness gradient. Med Eng Phys. 81:30–38.

Wang X, Xu S, Zhou S, Xu W, Leary M, Choong P, Qian M, Brandt M, Xie YM. 2016. Topological design and additive manufacturing of porous metals for bone scaffolds and orthopaedic implants: a review. Biomaterials. Mar. 83:127–141.

Wang YJ, Arabnejad Khanoki S, Tanzer M, Pasini D. 2018. Hip implant design with three-dimensional porous architecture of optimized graded density. J Mech Des. 140: 111406.

Yanez A, Cuadrado A, Martel O, Afonso H, Monopoli D. 2018. Gyroid porous titanium structures: a versatile solution to be used as scaffolds in bone defect reconstruction. Mater Des. 140:21–29.

Zadpoor AA. 2019. Additively manufactured porous metallic biomaterials. J Mater Chem B. 7(26):4088–4117.

Zhang L, Song B, Choi SK, Shi YS. 2021. A topology strategy to reduce stress shielding of additively manufactured porous metallic biomaterials. Int J Mech Sci. 197:15.

Zhu T, Cui Y, Zhang M, Zhao D, Liu G, Ding J. 2020. Engineered three-dimensional scaffolds for enhanced bone regeneration in osteonecrosis. Bioact Mater. 5(3): 584–601.